Atomic gas in debris discs

Antonio S. Hales,[1,2]★ M. J. Barlow,[3] I. A. Crawford[4] and S. Casassus[5,6]

[1]*Atacama Large Millimeter/Submillimeter Array, Joint ALMA Observatory, Alonso de Córdova 3107, Vitacura 763-0355, Santiago, Chile*
[2]*National Radio Astronomy Observatory, 520 Edgemont Road, Charlottesville, VA 22903-2475, USA*
[3]*Department of Physics and Astronomy, University College London, Gower Street, London WC1E 6BT, UK*
[4]*Department of Earth and Planetary Sciences, Birkbeck College London, Malet Street, London WC1E 7HX, UK*
[5]*Departamento de Astronomía, Universidad de Chile, Camino El Observatorio, 1515 Las Condes, Santiago, Chile*
[6]*Millennium Nucleus 'Protoplanetary Discs', Santiago 0000-0002-0433-9840, Chile*

ABSTRACT

We have conducted a search for optical circumstellar absorption lines in the spectra of 16 debris disc host stars. None of the stars in our sample showed signs of emission line activity in either Hα, Ca II or Na I, confirming their more evolved nature. Four stars were found to exhibit narrow absorption features near the cores of the photospheric Ca II and Na I D lines (when Na I D data were available). We analyse the characteristics of these spectral features to determine whether they are of circumstellar or interstellar origins. The strongest evidence for circumstellar gas is seen in the spectrum of HD 110058, which is known to host a debris disc observed close to edge-on. This is consistent with a recent ALMA detection of molecular gas in this debris disc, which shows many similarities to the β Pictoris system.

Key words: techniques: spectroscopic – circumstellar matter.

1 INTRODUCTION

Debris discs represent the final stage of the planet formation process. The dust observed in these systems is thought to be replenished through collisions between solid bodies (Wyatt 2008), and are therefore expected to be gas depleted. However, a few debris discs show the presence of small amounts of circumstellar gas. Whether this gas is remnant of the early disc stages (primordial) or of secondary origin (e.g. brought to the gas phase by photodesorption or by cometary activity) is a matter of contemporary debate (Dent et al. 2014; Moór et al. 2015; Greaves et al. 2016; Kóspál & Moór 2016; Kral et al. 2016; Lieman-Sifry et al. 2016; Marino et al. 2016).

Circumstellar gas was first discovered around β Pictoris over 40 yr ago when Slettebak (1975) noticed the presence of narrow Ca II absorption lines located at the centre of β Pic photospheric lines. Subsequent to the first imaging of the debris disc around β Pic by Smith & Terrile (1984), Hobbs et al. (1988) observed similar features both in Ca II and Na I. The radial velocities of the absorptions coincided with the radial velocity of the star, and were attributed to circumstellar gas orbiting the star. Variable absorption features have been identified, attributed to the evaporation of solid kilometre-sized bodies falling into the star (Beust et al. 1990; Crawford et al. 1994; Vidal-Madjar, Lecavelier des Etangs & Ferlet 1998; Kiefer et al. 2014a; Welsh & Montgomery 2016).

Over a dozen other debris discs with circumstellar gas absorption features have been identified with this method, such as HR 10 (Lagrange-Henri et al. 1990a), HD 32297 (Redfield 2007), 49 Ceti (Montgomery & Welsh 2012), HD 172555 (Kiefer et al. 2014b), HD 21620, HD 110411, HD 145964, HD 183324 (Welsh & Montgomery 2013) and ϕ Leo (Eiroa et al. 2016). Detecting gas in discs using absorption lines is difficult since the gas disc must be favourably oriented close to edge-on in order to be detected. On the other hand, the advantage of this method is that it is sensitive to much lower gas column densities compared to direct observations of gas emission.

In this work, we study the optical spectra of 16 debris disc host stars in order to search for gas-bearing β Pictoris-like systems. One of the main difficulties of this technique is to rule out interstellar (IS) absorption features, which may be very similar in profiles and strength to circumstellar lines. This requires careful analysis of the line characteristics (Lagrange-Henri et al. 1990b; Crawford, Beust & Lagrange 1998; Redfield 2007; Welsh & Montgomery 2013).

2 TARGET SAMPLE

The sample consists of 16 debris disc host stars taken from the catalogue of Mannings & Barlow (1998) having spectral types ranging from B8 to F7 (as listed in the Michigan Spectral Catalog for southern stars; Houk & Smith-Moore 1988). The sample was selected in terms of their low dust fractional luminosities, with all stars having $L_{IR}/L_\star$ values less than those investigated by Dunkin, Barlow & Ryan (1997) being selected in order to choose true

debris discs. Dust fractional luminosities were computed by fitting a blackbody to the observed spectral energy distributions (SED). The stellar SEDs were approximated using templates from the library of stellar atmospheres by Castelli & Kurucz (2004), for models with $\log g = 4.0$ and solar metallicity.

Fig. 1 shows the results from the SED fitting routine, where both the observed SED and the fitted *stellar + dust blackbody model* are plotted. $L_{IR}/L_\star$ values in our sample are found to range between 1.8 $\times 10^{-3}$ and 7.5 $\times 10^{-6}$. We estimate our method to be accurate to factors of 2–3 by comparing our $L_{IR}/L_\star$ results with values already published in the literature (Sylvester & Mannings 2000; Moór et al. 2006; Hales et al. 2014).

Based on their dust fractional luminosities, these systems are expected to be in a more advanced evolutionary stage than the sample studied by Dunkin et al. (1997). All stars have *Hipparcos* distances available (van Leeuwen 2007). Spectral standards of three spectral types were also observed in order to allow for spectral classification and removal of telluric absorption lines. Table 1 summarizes the properties of our sample, where we have listed the properties of our observed target sample along with those of the three observed spectral standards (HR 5558, HR 5670 and HR 6045).

3 OBSERVATIONS AND DATA REDUCTION

3.1 AAT/UCLES observations

Optical echelle spectroscopy of the 16 debris disc host stars was obtained using the UCL Echelle Spectrograph (UCLES) at the 3.9 metre Anglo–Australian Telescope (AAT). All observations were taken on the night of 2000 May 20. A log of the observations is given in Table 2, including the slit-width and seeing values. The 31.6 g mm^{-1} grating was used in conjunction with the MIT/LL CCD. Observations were carried out with two wavelength settings in order to cover the blue region of the spectra between 3834 and 5440 Å, and between 5550 and 9900 Å in the red. The red observations were optimized for the study of H$_\alpha$, He I and the Na I D lines, whilst the blue exposures covered the Ca II K and H lines as well as several metallic lines in the 4000–5000 Å region. The spectral resolution, estimated from measuring the FWHM of Thorium–Argon arc lines, was 0.115 Å ($\sim$8.8 km s^{-1}) at Ca II K (3933.663 Å), corresponding to a resolving power of $R = 34\,200$. At the location of the Na I D lines in the red part of the spectrum (5889.951 Å), the spectral resolution and resolving power were found to be 0.171 Å and $R = 34\,600$, respectively.

Overscan correction, dark subtraction and flat-fielding were performed using the Image Reduction and Analysis Facility (IRAF[1]) package developed by the National Optical Astronomy Observatory (NOAO). When more than one exposure for the same star was available, the different frames were co-added and the average taken. At this stage, the 'crreject' task was used in order to remove cosmic rays. Echelle spectra were extracted following standard echelle reduction procedures using the different tasks of the echelle package in IRAF. These include order tracing, extracting and blaze correcting each order. Wavelength calibration was performed using reference arc lines from a Thorium–Argon lamp. Each order was wavelength calibrated individually, producing a dispersion accuracy always better than 0.004 Å.

3.2 Magellan/MIKE observations

Follow-up observations of the target HD 110058 were obtained using the Magellan Inamori Kyocera Echelle (MIKE) spectrograph (Bernstein et al. 2003), mounted on the Magellan II telescope. In order to characterize the distribution of IS material in the surroundings of HD 110058, three stars located in the same direction and within a small range of distances from the main target were observed.

All observations were carried out in the night of 2008 July 4 under clear sky conditions and with seeing between 0.9 and 1.2 arcsec. The summary of the observations together with the target properties are shown in Table 3. MIKE allows us to obtain both the red and blue side of the spectrum simultaneously, covering from 3350 to 9150 Å. The 0.7×5 arcsec^2 slit was used that provided spectral resolutions of 42 000 and 32 000 in the blue and red parts of the spectra, respectively (as measured by fitting the FWHM of the Thorium–Argon lamp lines). All targets are bright ($V < 8$), so signal-to-noise ratios (S/N) higher than 15 can be obtained in both the blue and red arms in only a few minutes of total integration time (listed in the last two columns of Table 3).

Data reduction was performed using the CarPy MIKE data reduction package (Kelson 2003), which performs the standard steps for echelle reduction, i.e. overscan subtraction, order tracing, sky subtraction, extraction and wavelength calibration. The pipeline also combines multiple frames of the same target and to produce final combined spectra.

4 SPECTRAL CLASSIFICATION AND STELLAR PARAMETERS

In order to check the accuracy of previous spectral classifications of our sources, several regions of the blue parts of the acquired spectra were compared to those of the observed standards (as listed in Table 1) and also to archive spectra from the UVES Paranal Observatory Project (UVES POP; Bagnulo et al. 2003). The latter provides a library of high-resolution spectra of stars across the Hertzsprung–Russell Diagram at a resolution of $R \sim 80\,000$, which were degraded to the resolution of our UCLES spectra. Several regions of the 4000–5000 Å part of the observed spectra of the stars were compared by eye to the spectra of the nearest spectral types. In some cases, the template spectra were artificially broadened in order to match the rotational velocity of the star to be classified. No discrepancies between the Michigan spectral types of the target stars and their corresponding spectral templates were found, leading us to conclude that all of our stars have their previous Michigan Spectral Catalog classification confirmed. In cases when the Michigan Spectral Catalog had an uncertainty of the order of 1 or 2 spectral sub-classes, our method was able to discriminate and associate the star with one of those spectral types, as listed in Table 4.

In the case of the five F-type stars (and the A9 star HD 99211), whose spectra are rich in metallic species, radial velocities ($V_\odot$) were derived by cross-correlating the observed spectra with template spectra for stars of similar spectral type from the UVESPOP data base, for which radial velocities had already been measured. The FXCORR task in IRAF was used for this purpose, which allows one to cross-correlate several echelle orders simultaneously, providing a very accurate determination of $V_\odot$. This is reflected in the small error estimates presented in Table 4, which correspond to the standard deviation of the velocities obtained in the different orders. For the case of the late B-type and early A-type stars, these stars have intrinsically fewer metallic lines that can be used for radial velocity estimations. Therefore, the most prominent photospheric
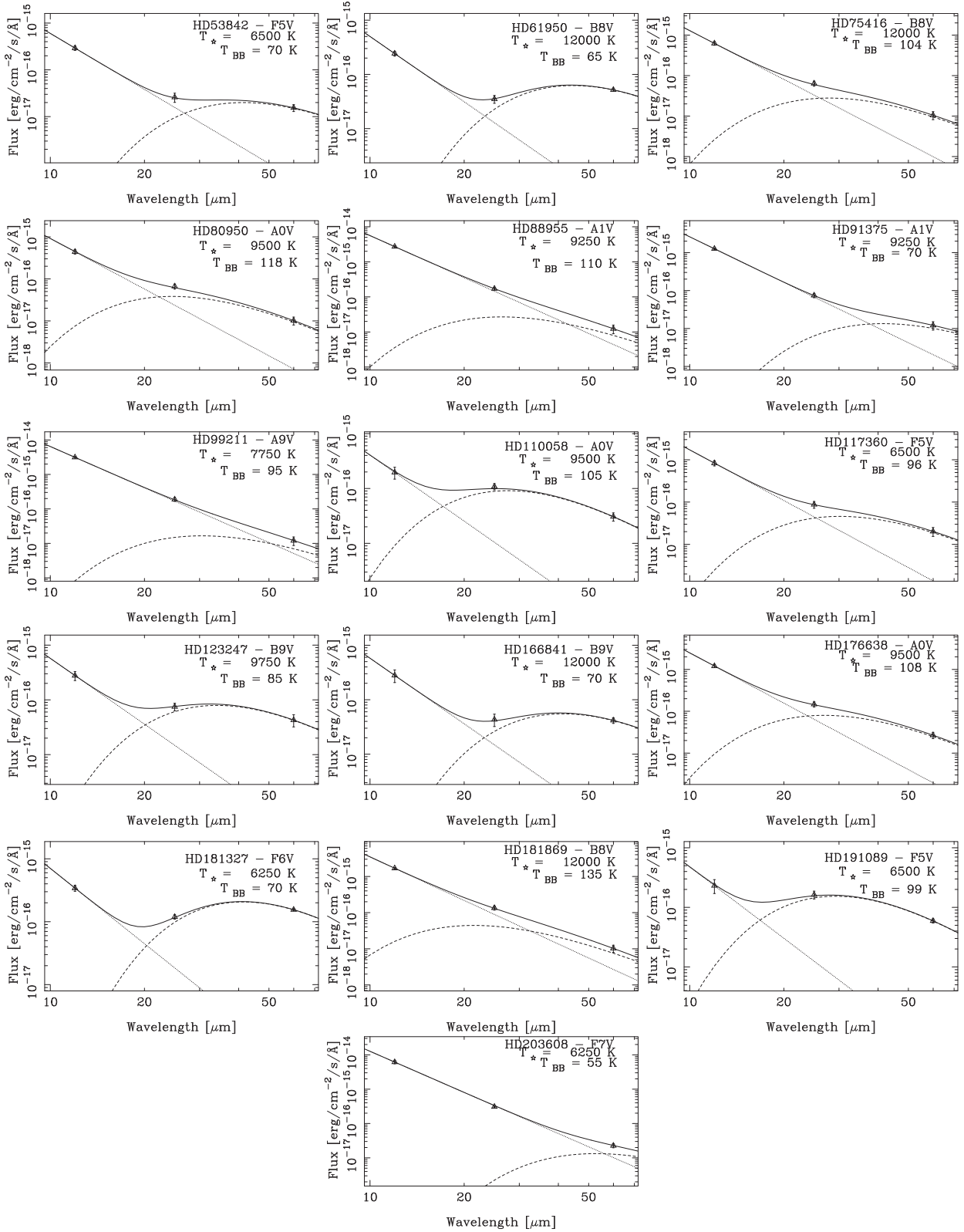
Figure 1. Dust blackbody fits to the infrared excesses used in the derivation of $L_{IR}/L_{\star}$ values for stars with different spectral types in our sample. The observed *IRAS* fluxes, as listed in Mannings & Barlow (1998), are plotted in blue with error bars denoting the 1σ photometric errors. The dotted line in red corresponds to the reference stellar SED from Castelli & Kurucz (2004), normalized to the 12 μm flux. The dashed line represents the fitted blackbody and the solid line represents the resulting SED (SED$_{\star}$+SED$_{DustBlackbody}$) that provides a satisfactory fit to the data. The stellar temperatures characteristic of the corresponding stellar model from the Castelli & Kurucz (2004) library and the temperature of the fitted blackbody are indicated in each plot.

Table 1. Debris disc host stars observed along with spectral standards used for spectral classification. Spectral types are from Michigan Spectral Catalogue (Houk & Smith-Moore 1988) and distances are derived from parallax measures listed in the *Hipparcos* catalogue (van Leeuwen 2007). $B-V$ colours are taken from the Simbad data base. The $L_{IR}/L_\star$ values were derived using the 25 and 60 μm *IRAS* excess fluxes. $L_\star$ is the luminosity of the Castelli & Kurucz (2004) stellar model, normalized to the 12 μm flux. L_{IR} is the bolometric luminosity of the blackbody that fits the infrared excesses.

Star	Other name	Previous spectral type	V	$(B-V)$	Distance (pc)	$L_{IR}/L_\star$	$L_\star$ ($L_\odot$)	Age (Myr)	References for age
HD 53842		F5V	7.46	0.460	57.3	2.6×10^{-4}	5.0	–	–
HD 61950		B8V	6.89	−0.028	362.3	1.4×10^{-4}	1121.8	–	–
HD 75416	η Cha	B8V	5.46	−0.094	96.9	1.8×10^{-5}	206.8	8	0
HD 80950		A0V	5.87	−0.016	80.8	6.6×10^{-5}	48.8	80	1
HD 88955	q Vel	A1V/A2V	3.84	0.063	31.5	7.5×10^{-6}	41.7	300	1
HD 91375		A1V	4.72	0.042	79.4	1.3×10^{-5}	123.4	265	1
HD 99211	γ Crt	A9V	4.08	0.216	25.7	1.1×10^{-5}	18.8	600	2
HD 110058		A0V	7.98	0.148	107	2.0×10^{-3}	33.0	17	5
HD 117360	S Cha	F5V/F6V	6.48	0.480	35.1	1.5×10^{-4}	5.4	–	–
HD 123247		B9.5V/B9V	6.43	0.000	101.1	2.4×10^{-4}	52.3	–	–
HD 166841		B8V/B9V	6.32	−0.030	213.7	1.1×10^{-4}	450.8	–	–
HD 176638	ζ CrA	B9V/A0V	4.75	−0.027	56.3	5.1×10^{-5}	64.4	–	–
HD 181327		F5V/F6V	7.04	0.480	50.6	2.4×10^{-3}	4.1	12^{+8}_{-4}	3
HD 181869	α Sgr	B8V	3.95	−0.083	52.1	7.9×10^{-6}	161.4	110^3	1
HD 191089		F5V	7.17	0.480	53.5	1.8×10^{-3}	3.5	12^{+8}_{-4}	3
HD 203608	γ Pav	F7V/F6V	4.22	0.494	9.2	1.0×10^{-5}	2.4	10^3	4
HR 5558	β Cir	A0V	5.32	0.044	75.8	–	–	–	–
HR 5670		A3V	4.06	0.100	29.6	–	–	–	–
HR 6045	θ Nor	B8V	5.12	−0.104	90.4	–	–	–	–

References: (0) Mamajek, Lawson & Feigelson (1999), (1) Rieke et al. (2005), (2) Song et al. (2001), (3) Moór et al. (2006), (4) Bryden et al. (2006), (5) Kasper et al. (2015).

lines of Ca II, Mg II and Fe I were used for performing Gaussian fitting to the centres of the photospheric lines. The heliocentric $V_\odot$ values listed in Table 4 for these stars correspond to the mean obtained using the different lines. The Mg II doublet at 4481.13 and 4481.33 Å is unresolved in the case of the B- and early A-type stars, and therefore, was not used for radial velocity determination. Earth radial velocity corrections were applied to each spectral range in order to obtain heliocentric velocities [obtained using the radial velocity (RV) Starlink package].

Projected rotational velocities ($v \sin i$) were derived using the STAROT package within DIPSO, which allows us to artificially broaden the spectrum of a stellar template to match the spectra of the observed star. Template spectra with previously measured $v \sin i$ values for each spectral type were taken from the UVESPOP data base, by selecting the stars with the lowest rotational velocities. Artificial broadening was then applied until a satisfactory fit to the observed spectra was achieved. Derived rotational velocities for our target stars are presented in column 3 of Table 4.

5 EVIDENCE FOR CIRCUMSTELLAR GAS

Of the 16 targets observed, 4 are found to exhibit narrow absorption features located near the centre of the photospheric Ca II H & K lines – these stars are HD 61950, HD 75416, HD 110058 and HD 166841. Similar absorption features are seen in the Na I D lines, with the exception of HD 61950 and HD 75416, for which only Ca II data were available. No narrow absorption components can be seen in either the Ca II K or Na I D line profiles of the remaining stars of our sample. In addition, a narrow feature was also detected in the Ca II H & K spectrum of the spectral standard HR 5558. Fig. 2 shows the H & K regions of HD 61950 and HD 75416 in the heliocentric velocity frame, with the radial velocities of the stars marked by a vertical line. Figs 3, 4 and 5 shows the Na I D and the Ca II H & K lines of HD 110058, HD 166841 and HR 5558 in

the heliocentric velocity frame. These features are too narrow to be photospheric in nature and therefore they must be produced by absorption of stellar light by either an IS or circumstellar gas cloud. There is a good correspondence between the radial velocities of the components from the different species, as is expected if both the calcium and sodium are located in the same cloud. For both HD 110058 and HD 166841, there is a strong absorption component that coincides, within the errors, with the radial velocity of the star. HD 61950 and HD 75416 have components that partially overlap the stellar radial velocity, while in the case of HR 5558, the velocity of the absorption feature is totally dissimilar to that of the star and is deemed to be IS in origin (see Section 5.3.5).

The fact that the radial velocities of both the star and the absorbing cloud are similar is not a sufficient condition to rule out that the absorption lines detected are of IS origin. There is not a unique criterion that may be used in order to discriminate between an IS or circumstellar origin for absorption features, instead, it is common to refer to a set of criteria that can be used together in order to resolve the nature of the absorption features (Dunkin et al. 1997). To rule out an IS origin for an absorption feature, one has to consider the following:

(i) Is the radial velocity of the narrow absorption feature the same as the stellar velocity?

(ii) Is the radial velocity of the narrow absorption consistent or not with known IS velocities in the same direction?

(iii) Is the observed N(Ca II)/N(Na I) column density ratio consistent with circumstellar (usually >1) or IS (usually <1) values?

(iv) Is the absorption observed towards stars in the similar line of sight?

The N(Ca II)/N(Na I) must, however, be treated with care as low-density clouds or shocked shells in the IS medium have also been found to exhibit N(Ca II)/N(Na I) > 1 (e.g. Crawford 1991; Smoker, Keenan & Fox 2015).

Table 2. Log of UCLES observations.

Object	RA (J2000)	Dec (J2000)	Airmass	Seeing (arcsec)	Exposure (s)	Central wavelength (Å)	Slit width (arcsec)	Slit length (arcsec)
HD 53842	06:46:00.45	−83:59:35.2	1.780	1.5	1000	4400.03	1.47	6.96
			1.803	1.5	1000	4400.03	1.47	6.96
			1.832	1.5	1000	4400.03	1.47	6.96
			2.249	2.5	400	6699.95	1.47	5.6
HD 61950	07:36:16.97	−69:03:29.6	1.384	1.5	750	4400.03	1.47	6.96
			1.413	1.5	750	4400.03	1.47	6.96
			3.699	2.5	350	6699.95	1.47	5.6
HD 75416	08:41:14.77	−78:57:55.3	1.496	1.5	250	4400.03	1.47	6.96
			1.501	1.5	250	4400.03	1.47	6.96
			2.348	2.5	200	6699.95	1.47	5.6
HD 80950	09:17:24.97	−74:44:09.9	1.384	1.5	500	4400.03	1.47	6.96
			2.447	2.5	200	6699.95	1.47	5.6
HD 88955	10:14:44.29	−42:07:21.1	1.080	1.5	100	4400.03	1.47	6.96
			2.438	2.5	50	6699.95	1.47	5.6
HD 91375	10:30:18.21	−71:59:40.1	1.353	1.5	200	4400.03	1.47	6.96
			2.195	2.5	60	6699.95	1.47	5.6
HD 99211	11:24:53.33	−17:41:05.1	1.043	1.5	150	4400.03	1.47	6.96
			2.188	2.5	40	6699.95	1.47	5.6
HD 110058	12:39:46.24	−49:11:54.5	1.475	1.5	1000	4400.03	1.47	6.96
			1.471	1.5	1000	4400.03	1.47	6.96
			1.473	1.5	1000	4400.03	1.47	6.96
			1.345	2.5	1000	6699.95	1.47	5.6
HD 117360	13:33:10.61	−77:34:13.7	1.446	2.5	800	4400.03	1.47	6.96
			1.446	2.5	800	4400.03	1.47	6.96
			1.625	3.0	400	6699.95	1.47	5.6
HD 123247	14:07:40.85	−48:42:14.8	1.048	2.5	1000	4400.03	1.47	6.96
HD 166841	18:17:59.57	−68:13:46.0	1.318	2.3	800	4400.02	1.47	7.0
			1.256	3.0	400	6699.95	1.47	5.6
HD 176638	19:03:06.95	−42:05:39.6	1.075	2.3	250	4400.02	1.47	7.0
			1.048	3.0	80	6699.95	1.47	5.6
HD 181327	19:22:58.63	−54:32:17.2	1.127	2.0	900	4400.02	1.47	7.0
			1.150	2.0	900	4400.02	1.47	7.0
			1.119	2.3	400	6699.95	1.47	5.6
HD 181869	19:23:53.25	−40:36:56.3	1.024	2.3	100	6699.95	1.47	5.6
			1.114	2.0	100	4400.02	1.47	7.0
			1.039	2.3	40	6699.95	1.47	5.6
HD 191089	20:09:05.54	−26:13:23.1	1.013	2.3	1000	4400.02	1.47	7.0
			1.005	2.3	1000	4400.02	1.47	7.0
			1.470	2.3	400	6699.95	1.47	5.6
			1.087	2.3	400	6699.95	1.47	5.6
HD 203608	21:26:25.91	−65:21:56.9	1.207	2.0	200.0	4400.02	1.47	7.0
			1.357	2.3	100	6699.95	1.47	5.6
HR 5558	14:55:44.86	−33:51:19.9	1.006	2.5	500	4400.03	1.47	6.96
			1.164	3.0	120	6699.95	1.47	5.6
HR 5670	15:17:30.36	−58:48:04.9	1.134	2.5	200	4400.03	1.47	6.96
			1.225	3.0	40	6699.95	1.47	5.6
HR 6045	16:15:15.23	−47:22:17.4	1.085	2.5	400	4400.03	1.47	6.96
			1.048	2.5	100	6699.95	1.47	5.6

When multiple epoch observations are available, one can also study variability of the absorption features, as circumstellar lines often vary with time (Beust et al. 1998; Redfield, Kessler-Silacci & Cieza 2007; Welsh & Montgomery 2013). However, not all circumstellar lines are variable, as for instance in β Pic, the strongest component is stable and corresponds to the main disc absorption (as opposed to the variable components that are interpreted as evaporating comets; Beust et al. 1998).

We measured the equivalent widths and radial velocities of the narrow absorption features on the normalized spectra by using the

Table 3. Summary of MIKE observations. Spectral types are from the Michigan Spectral Catalog. Distances are derived from *Hipparcos* parallaxes. Column 6 denotes the angular separation from the direction of HD 110058.

Object	RA (J2000)	Dec (J2000)	Spectral type	V	Distance (pc)	Angular separation	Integration time (s)	S/N (blue/red)
HIP 61557	12:36:46.60	−50:20:07.42	A0V	6.39	102	1°.2	198	40/30
HD 110058	12:39:46.24	−49:11:55.54	A0V	7.98	107	0°	480	25/21
HIP 61342	12:34:08.84	−50:03:36.95	A3V	7.23	115	1°.3	120	17/15
HIP 60360	12:22:36.52	−49:19:34.07	A2IV/V	7.94	123	2°.8	207	17/15

Table 4. Measured parameters of the debris disc host stars. Column 2 confirms the previous spectral classification for all of our targets. Columns 3 and 4 list the projected rotational velocities ($v \sin i$) and the heliocentric radial velocities ($V_\odot$), respectively. The uncertainties quoted for $V_\odot$ and $v \sin i$ correspond to the dispersion obtained when deriving the quantities using the different lines.

Star	Spectral type	$v \sin i$ (km s^{-1})	$V_\odot$ (km s^{-1})
HD 53842	F5V	24 ± 2	10 ± 1
HD 61950	B8V	240 ± 9	20 ± 5
HD 75416	B8V	290 ± 2	15 ± 5
HD 80950	A0V	80 ± 4	14 ± 3
HD 88955	A1V	100 ± 4	7 ± 3
HD 91375	A1V	15 ± 2	8 ± 3
HD 99211	A9V	110 ± 2	−1 ± 2
HD 110058	A0V	180 ± 4	12 ± 3
HD 117360	F5V	11 ± 2	−33 ± 1
HD 123247	B9V	140 ± 4	7 ± 3
HD 166841	B9V	245 ± 8	0 ± 3
HD 176638	A0V	260 ± 6	−27 ± 3
HD 181327	F6V	22 ± 2	−1 ± 1
HD 181869	B8V	55 ± 9	−4 ± 5
HD 191089	F5V	33 ± 2	−6 ± 1
HD 203608	F6V	3 ± 1	−30 ± 1
HR 5558	A0V	180 ± 4	1 ± 3
HR 5670	A3V	95 ± 4	9 ± 2
HR 6045	B8V	205 ± 5	1 ± 4

Figure 2. Heliocentric velocity plots of the narrow Ca II H (dotted line) and K (solid line) absorption components present in the spectra of HD 61950 and of HD 75416. The vertical lines denote the radial velocity of the star. The H line spectra have been shifted vertically for plotting purposes.

Emission Line Fitting (ELF) Starlink routine, which fits Gaussian profiles to the absorption features and returns the equivalent width and centre of these unsaturated components. Table 5 presents the derived equivalent widths and radial velocities of the narrow Ca II and Na I absorption features present in the spectra of our targets.

5.1 Cloud modelling

The Voigt Absorption Profile/Interstellar Dabbler software for modelling IS absorption lines (VAPID; Howarth et al. 2002), was used to estimate the column density (N), radial velocity (v) and the velocity dispersion (b) of the material causing the observed absorption in the Ca II K and Na I D$_2$ lines. VAPID assumes a Gaussian line-of-sight velocity distribution for each absorbing cloud, and uses Voigt functions and least-squares optimization to estimate cloud parameters of the many cloud components required to reproduce the observed spectra. Uncertainties in the resulting parameters are estimated using a Monte Carlo method to derive confidence intervals in the parameter space. Oscillator strengths of 0.635 and 0.631 were assumed for the Ca II K and Na I D$_2$ lines, respectively (Morton 1991).

The best-fitting model parameters that were found to reproduce successfully the data are presented in Table 6, while models versus data are plotted in Figs 6 and 7.

5.2 Velocity projections of known IS clouds/shells

All the stars in this study lie in the Fourth Galactic Quadrant. This region is almost entirely occupied by the Scorpius–Centaurus association, extending between ∼290° and 360° in longitude and being the closest OB association with the Sun (Blaauw 1964; de Geus et al. 1989). Three subgroups have been identified to reside within this association: the Upper Centaurus-Lupus (UCL), Lower Centaurus-Crux (LCC) and the Upper Scorpius (US) shells (de Geus 1992). These subgroups have been studied extensively, and the IS medium in their proximity has been modelled as expanding spherical shells of gas, whose physical parameters such as shell centre, radius and expansion velocity have been derived by
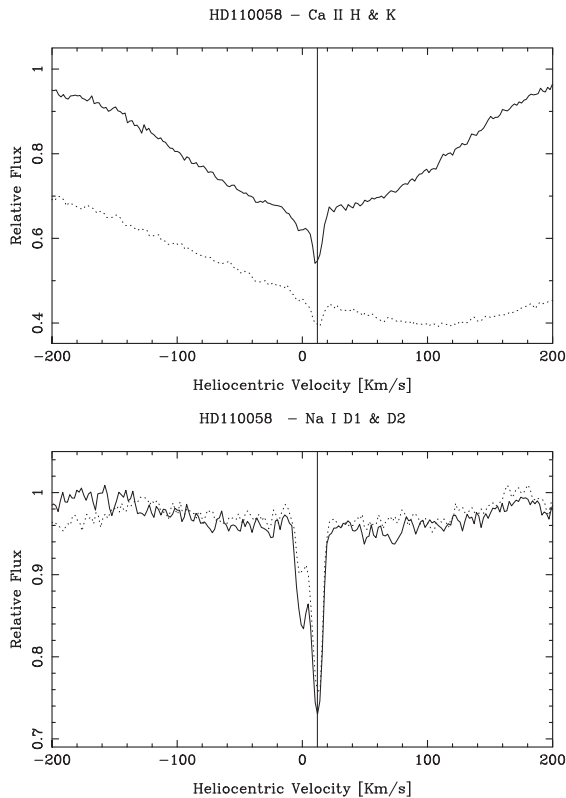
Figure 3. Heliocentric velocity plots of narrow absorption features seen towards HD 110058 both in the Ca II H & K lines (top panel) and in the Na I D lines (bottom panel). The solid lines correspond to the Ca II K and Na I D_2 lines. The Na I region of the spectra was divided by the spectrum of the B8 spectral standard HR 6045 in order to remove telluric absorption features.
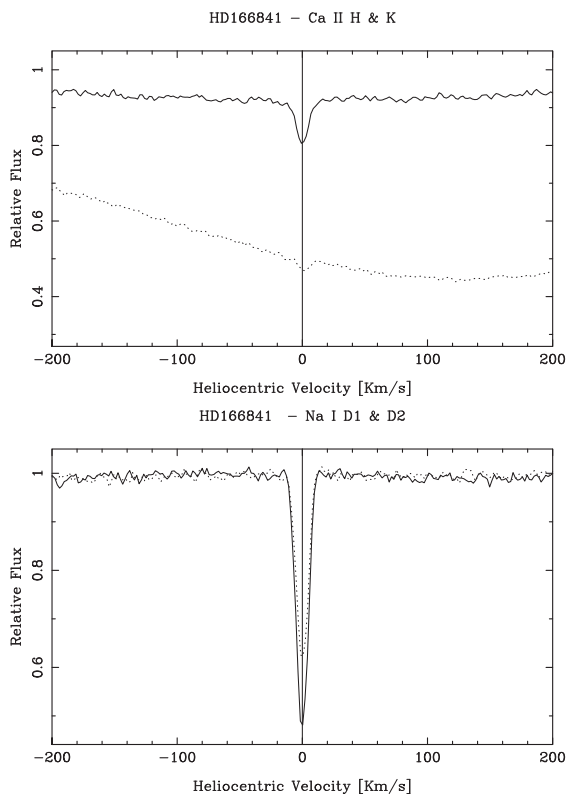

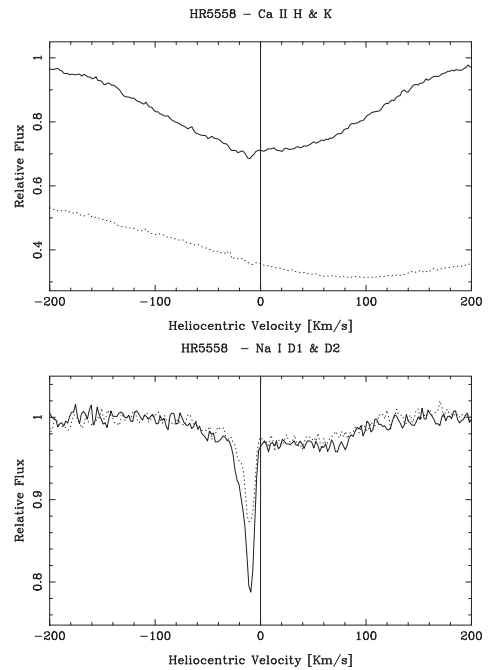**Figure 4.** Same as Fig. 3 for HD 166841.

Figure 5. Same as Fig. 3 for spectral standard HR 5558.

de Geus et al. (1989), de Geus (1992) and de Zeeuw et al. (1999). The location of our target stars with respect to the UCL, LCC and US shells are plotted in Fig. 8.

In addition to the UCL, LCC and US shells, one must also consider the structure of the local IS medium including the Local Interstellar Cloud (LIC; Redfield & Linsky 2015). The LIC is a warm, low-density IS cloud that is itself located within a hot Local Cavity in the IS medium that extends to approximately 50 pc (Welsh et al. 2010). The LIC is thought to move in the direction $l = 186° \pm 3$, $b = -16° \pm 3$, with a heliocentric velocity of $v = 26 \pm 1$ km s^{-1} (Lallement et al. 1995). The Local Cavity is thought to contain several small clouds located within a few tens of parsecs of the Sun, with characteristics similar to the LIC. One such possible cloud is the 'G' cloud, which appears to move at $v = 29 \pm 1$ km s^{-1} in the direction $l = 184°.5 \pm 2.3$ and $b = -20°.5 \pm 1.8$ (Lallement et al. 1992).

5.2.1 The LIC and G clouds

Given an IS cloud moving with velocity v_w in a direction (l_w, b_w), the line-of-sight velocity component of the cloud in a direction (l, b) is given by (Crutcher 1982):

$$\frac{v}{v_w} = \sin b \cdot \sin b_w + \cos b \cdot \cos b_w \cdot \cos(l - l_w), \qquad (1)$$

where the terms on the right-hand side correspond to the cosine of the angle between (l, b) and (l_w, b_w).

5.2.2 The UCL, LCC and US shells

For an expanding shell model, the following equation can be used to determine the velocity component for a point (l, b) on the surface of a sphere of radius r_s, centred at a distance R from the Sun at (l_o, b_o) (e.g. Crawford 1991):

$$v = \pm \frac{v_o}{r_s} \sqrt{R^2(\cos \theta^2 - 1) + r_s{}^2}, \qquad (2)$$

Table 5. Equivalent widths and heliocentric velocities of the narrow absorption lines observed in the spectra of the target stars. The equivalent widths are in mÅ. For stars where two entries are listed, these correspond to separate velocity components.

| Star | Ca II K | | Ca II H | | Na I D$_1$ | | Na I D$_2$ | |
	EW (mÅ)	$V_\odot$ (km s^{-1})	EW (mÅ)	$V_\odot$ (km s^{-1})	EW (mÅ)	$V_\odot$ (km s^{-1})	EW (mÅ)	$V_\odot$ (km s^{-1})
HD 61950	27.1 ± 2.1	8.3 ± 0.4	12.2 ± 2.7	8.8 ± 0.7	–	–	–	–
	14.2 ± 1.9	17.9 ± 0.8	6.3 ± 2.1	17.1 ± 0.9	–	–	–	–
HD 75416	2.5 ± 1.1	−7.9 ± 3.1	–	–	–	–	–	–
	2.7 ± 0.5	6.9 ± 0.5	–	–	–	–	–	–
	1.3 ± 0.7	17.2 ± 1.8	–	–	–	–	–	–
HD 110058	13.9 ± 2.1	−1.2 ± 0.5	5.8 ± 2.5	−2.4 ± 0.6	11.3 ± 1.5	−1.4 ± 0.9	28.7 ± 2.2	−0.3 ± 0.8
	22.3 ± 1.3	11.8 ± 0.1	19.6 ± 1.9	11.9 ± 0.3	45.5 ± 4.9	12.9 ± 0.7	46.9 ± 5.2	12.0 ± 0.5
HD 166841	20.1 ± 1.7	0.1 ± 0.2	6.1 ± 2.1	1.5 ± 0.4	93.1 ± 9.7	−0.1 ± 0.3	134.4 ± 6.9	−0.1 ± 0.2
HR 5588	–	–	–	–	4.2 ± 1.1	−17.1 ± 4.9	13.1 ± 0.9	−17.4 ± 3.8
	4.7 ± 1.1	−10.3 ± 0.9	–	–	20.5 ± 3.2	−10.5 ± 0.8	33.3 ± 4.5	−10.2 ± 0.6

Table 6. Derived line profile parameters for narrow Ca K and Na D$_2$ velocity components derived from VAPID modelling. The parameter errors reported represent the 1σ dispersion in each parameter (i.e. single-parameter 68 per cent confidence intervals). The last column gives the N(Ca II)/N(Na I) ratio.

| Star | Ca K | | | Na D$_2$ | | | N(Ca II)/N(Na I) |
	$V_\odot$ (km s^{-1})	b (km s^{-1})	log N (cm^{-2})	$V_\odot$ (km s^{-1})	b (km s^{-1})	log N (cm^{-2})	
HD 61950	8.3 ± 0.4	1.9 ± 0.6	11.56 ± 0.03	–	–	–	–
	18.1 ± 0.7	3.6 ± 1.2	11.32 ± 0.05	–	–	–	–
HD 75416	−10.2 ± 1.8	9.2 ± 2.0	10.46 ± 0.06	–	–	–	–
	6.9 ± 0.4	0.3 ± 0.1	10.67 ± 0.02	–	–	–	–
	18.5 ± 1.4	0.2 ± 0.5	10.20 ± 0.04	–	–	–	–
HD 110058	−1.4 ± 0.4	5.7 ± 0.9	11.19 ± 0.03	−0.1 ± 0.2	2.1 ± 0.7	11.19 ± 0.02	1.00
	11.8 ± 0.2	0.8 ± 0.1	11.73 ± 0.03	12.2 ± 0.1	2.0 ± 0.4	11.53 ± 0.02	1.41
HD 166841	0.1 ± 0.1	4.4 ± 0.4	11.40 ± 0.02	−0.25 ± 0.1	3.5 ± 0.2	12.01 ± 0.02	0.25
	−16.5 ± 1.9	3.9 ± 3.4	10.43 ± 0.11	–	–	–	–
HR 5588	–	–	–	−19.1 ± 0.5	3.9 ± 0.9	10.87 ± 0.04	–
	−10.4 ± 0.4	0.4 ± 0.3	10.70 ± 0.02	−9.6 ± 0.2	0.6 ± 0.1	11.69 ± 0.02	0.1

where $\cos\theta$ is given by the term in the right-hand side of equation (1) (substituting (l_w, b_w) for (l_o, b_o)), θ is the angle between (l, b) and (l_o, b_o) and v_o is the expansion velocity with respect to the local standard of rest (LSR) or V_{LSR}. Conversion from LSR to Heliocentric velocities was performed using the RV Starlink package. We used equations (1) and (2) to calculate the projected velocity components for the different IS clouds and shells in the direction of our targets with detected absorption, which are presented in Table 7.

5.3 Discussion of individual stars

5.3.1 HD 61950

HD 61950 is a B8 dwarf that shows a distinctive two-component absorption feature seen in both the Ca H and K lines. The absorption components are centred at +8.3 and +18.1 km s^{-1}, lying near the base of the broad photospheric line. The redmost component, at +18.1 ± 0.7 km s^{-1} coincides within the errors with the star's heliocentric velocity (20 ± 5 km s^{-1}), although there is quite a large uncertainty on the latter due to the lack of prominent metallic lines on the spectrum of this B-type star. The Ca II equivalent width ratio suggests that for both narrow components the line is unsaturated, as the derived K:H EW ratio is ∼2 in both cases (a Ca II K:H ratio of 2 is expected in the case of unsaturated lines, as the oscillator strength of the H line is half that of the K line).

Given that HD 61950 is the most distant star in our sample (d = 362 pc), it is more probable that these features are of IS origin.

The velocity projections of known clouds and shells predict that the UCL shell should contribute an absorption feature at +9.4 km s^{-1} (Table 7) that coincides extremely well with the main absorption component seen at +8.3 km s^{-1}.

Comparison with Ca II K observations towards stars in similar directions suggests that both components in the spectrum of HD 61950 are IS. The LSR velocities of the two narrow Ca II absorption components seen towards HD 61950 ($l = 281°$, $b = −21°$, $d = 362$ pc) correspond to −3.7 and +5.9 km s^{-1}. Hunter et al. (2006) detected two Ca II K absorption components towards HD 76131 ($l = 273°$, $b = −7°$, $d = 453$ pc) at LSR velocities of −2 and +8 km s^{-1}, with EWs of 110 and 21 mÅ, respectively. These two velocity components are also detected in the spectra of HD 67536 ($l = 276°$, $b = −16°$, $d = 450$ pc), at LSR velocities of −4 and +5.3 km s^{-1} with EW of 16 and 11 mÅ, respectively. The LSR velocities of the two components detected towards HD 61950 coincide with the range of velocities of the two IS clouds reported by Hunter et al. (2006) are detected. It is therefore very likely that both absorption features seen towards HD 61950 are IS in nature.

5.3.2 HD 75416

HD 75416 (η Cha) lies at a distance of 97 pc and is also a B8V star. It is the brightest member of the 8 Myr old η Cha cluster (Mamajek et al. 1999), and is the only debris disc in this young, disc-rich, stellar association (Sicilia-Aguilar et al. 2009). Gaussian modelling of the photospheric lines indicate that the star is a fast rotator
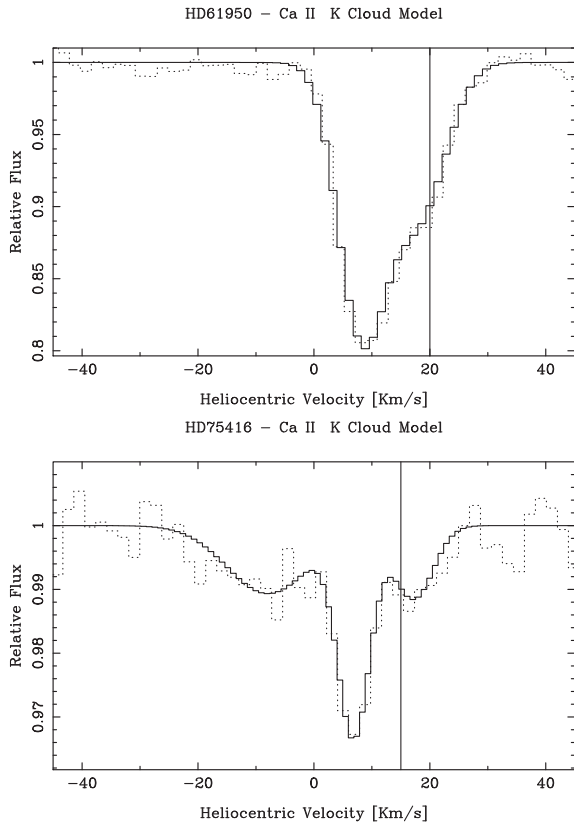
Figure 6. Cloud models for the Ca II K absorption features seen towards HD 61950 (top) and HD 75416 (bottom). The solid line shows the model that gives a satisfactory to the data (dotted line). The vertical line represents the heliocentric velocity of the star.

($v \sin i \sim$290 km s^{-1}), as was already noted by Sicilia-Aguilar et al. (2009), and that the stellar heliocentric velocity is +15 ± 5 km s^{-1} (in agreement with the V$_\odot$ = 14 ± 10 km s^{-1} value derived by de Bruijne & Eilers (2012)). A very weak absorption feature is detected at the centre of the photospheric Ca II K profile. Three separate components at heliocentric velocities of −10.2, +6.9 and +18.5 km s^{-1}, were required in order to satisfactorily fit the observed profile (Fig. 6). There is no evidence of corresponding features in the intrinsically weaker Ca II H line.

The cloud models imply very low calcium column densities, with the strongest components being the ones at −10.2 and +6.9 km s^{-1}. The velocity component observed at +6.9 km s^{-1} could be related to the UCL shell (velocity projection of +4.3 km s^{-1}); however, no known clouds/shells can account for the 18.5 km s^{-1} component. This feature is interesting because, despite being very weak (only 1.3 mÅ equivalent width), it lies close to the stellar velocity. However, the lack of additional information regarding this absorption feature makes it difficult to draw any conclusions regarding the nature of this feature. Additional observations of the Na I D region could help in resolving the origin of these features.

5.3.3 HD 110058

HD 110058 is an A0V star located at a distance of 107^{+10}_{-8} pc, in the direction of the LCC shell (van Leeuwen 2007). HD 110058 was first identified by Mannings & Barlow (1998) as a debris disc host

star. The disc was undetected at 1350 μm with SCUBA by Sylvester, Dunkin & Barlow (2001), which allowed them to estimate an upper limit to the dust mass of less than 5 × 10^{-6} M$_\odot$. Sylvester et al. (2001) estimate the fractional disc luminosity of 1.89 × 10^{-3}, in good agreement with our estimate of 2.0 × 10^{-3}. This is very similar to the dust fractional luminosity of β Pic (2.4 × 10^{-3}, Moór et al. 2011), and comparable to those of other A-type star debris disc around which circumstellar gas has been detected (Hughes et al. 2008; Moór et al. 2011; Dent et al. 2014; Moór et al. 2015; Lieman-Sifry et al. 2016; Marino et al. 2016).

Near-infrared Very Large Telescope/SPHERE imaging has revealed that, similar to β Pic, the debris disc around HD 110058 is seen very close to edge-on (Kasper et al. 2015). Recent ALMA observations confirm the near to edge-on inclination of the disc, and also show a 5σ detection of carbon monoxide towards the system (Lieman-Sifry et al. 2016).

There is some discrepancy in the literature regarding HD 110058's radial velocity. Moór et al. (2006) measured the radial velocity of HD 110058 to be +21.7 ± 1.3 km s^{-1}, while de Bruijne & Eilers (2012) estimate a radial velocity of 5 ± 1 km s^{-1}. Our measurement lies somewhere in between the estimates of Moór et al. (2006) and de Bruijne & Eilers (2012).

A strong, sharp, absorption component is detected in both the Calcium and Sodium regions at the very base of the photospheric line. Modelling of the absorption feature indicates that there are actually two velocity components, centred near −1 and +12 km s^{-1}, respectively. None of the known IS clouds/shells appear to have projections at these velocities and so cannot account for the observed features. The component near +12 km s^{-1} lies right at the stellar radial velocity of +12 ± 3 km s^{-1} we derived, which would argue for a circumstellar nature for this feature.

It is interesting to note that in the case of the +12 km s^{-1} component, the equivalent widths of the D$_1$ and D$_2$ lines are equal within the errors, suggesting saturation. The same effect is seen with regard to the H and K calcium lines. This could be explained by the presence of clumpy intervening material, similar to what has been modelled for β Pictoris (Lagrange-Henri et al. 1992). For both velocity components, the Ca II/Na I ratios that we derive are close to unity, and are the largest found in our sample. Redfield et al. (2007) note, however, that it is hard to differentiate a circumstellar from IS origin based on the abundance ratios alone, since a wide range of Ca II/Na I ratios are detected even locally. In their search for atomic absorption in nearby debris discs, Redfield et al. (2007) find that their best candidates for circumstellar absorption have Ca II/Na I ratios between 3.9 and 46.

The coincidence between the radial velocities of the narrow absorption feature and the star, the lack of known IS clouds/shells that can account for absorptions at these velocities, together with the Ca II/Na I ratio of $\sim$1 strongly argue for a circumstellar nature for the component seen at +12 km s^{-1}. The fact that the component seen at $\sim$12 km s^{-1} is saturated while the one at $\sim$−1 km s^{-1} is not, indicates that they have different column densities, suggesting that they may be different in nature.

The MIKE observations of HD 110058 and of reference stars in the vicinity of HD 110058 confirm that the feature at a lower velocity is IS. The feature is observed in all stars (Fig. 9), and its depth increases with distance as expected if the absorption is caused by interstellar material. On the other hand, the absorption feature at $\sim$12 km s^{-1} is detected only towards HD 110058. Therefore, we conclude that this absorption feature is indeed circumstellar.

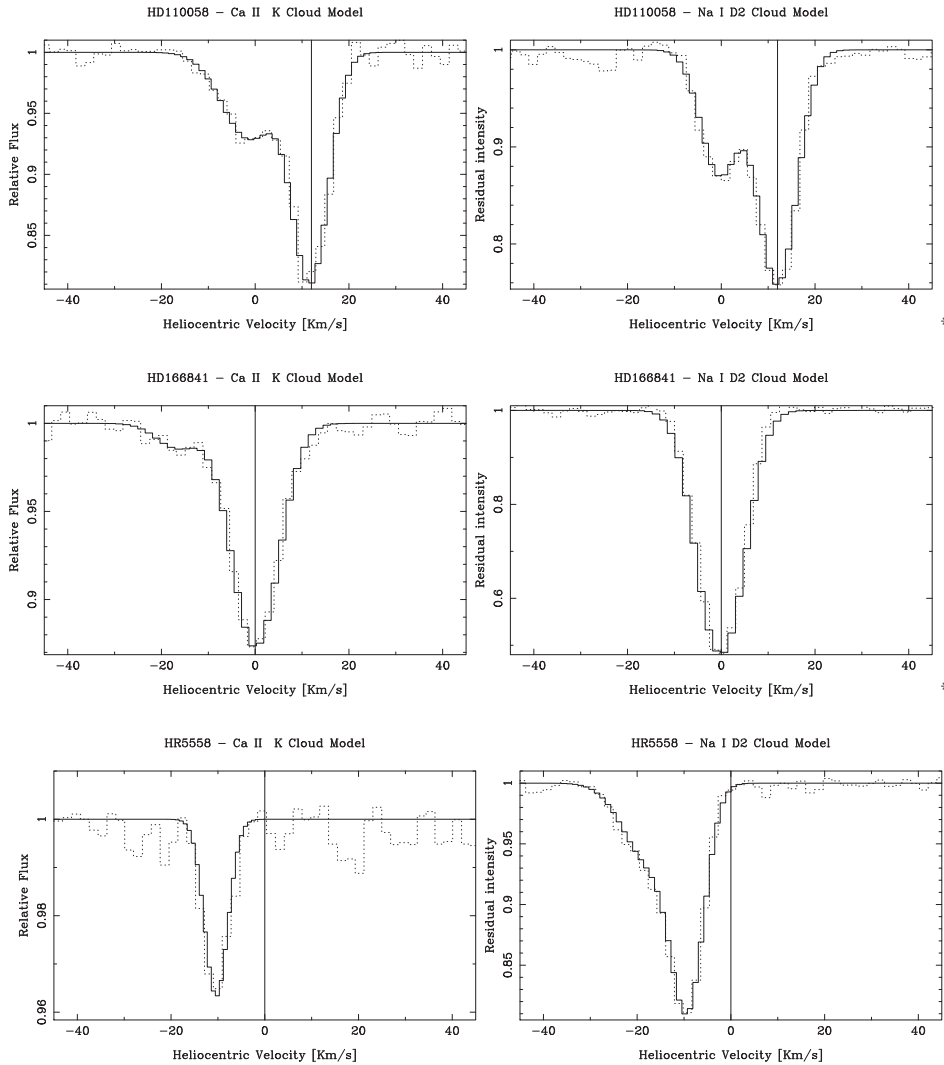**Figure 7.** Cloud models for the Na I D$_2$ (right-hand panel) and Ca II K (left-hand panel) absorption features seen towards HD 110058, HD 166841 and HR 5558. The solid line shows the model that gives a satisfactory fit to the data (dotted line). The vertical line represents the heliocentric velocity of the star.

5.3.4 HD 166841

HD 166841 is B9V star located 214 pc away from the Sun in the direction of the centre of the UCL shell. The star was first identified as a debris disc host by Mannings & Barlow (1998), but no further studies of this object have been carried out. The value of the projected rotational velocity that we derive (245 ± 8 km s^{-1}) is consistent with the star being of late B-type. Despite being a quite distant star, the $E(B - V)$ value we estimate assuming the normal colours of a B9V star is quite low ($E(B - V) = 0.02$).

A strong narrow absorption feature is easily seen right at the centre of the photospheric Ca II and Na I lines. Both the calcium and sodium absorption features are found to be located at $V_{\odot} = 0 \pm 1$ km s^{-1}, coinciding extremely well with the radial velocity of the star. The derived equivalent widths of the different components suggest that the lines are not saturated and the cloud modelling indicates that Ca II/Na I column density ratio is ∼0.3.

Although the velocity projections of known clouds/shells cannot be responsible for the observed absorption feature, we investigated the presence of similar absorption components in the spectra of stars in similar directions. The LSR velocity of the component seen towards HD 166841 ($l = 326°$, $b = −22°$, $d = 214$ pc) is

−1.8 km s^{-1}. Hunter et al. (2006) reports $+2.4 \pm 0.1$ km s^{-1} Ca II K component on the direction of HD 142758 ($l = 325°$, $b = −4°$, $d = 4000$ pc) with 65 mÅ equivalent width. Hunter et al. (2006) also detected two Ca II K absorption features in the spectrum of HD 143448 ($l = 324°$, $b = 6°$, $d = 520$ pc), at $−3.6 \pm 0.1$ km s^{-1} (EW = 18 mÅ) and $+2.0 \pm 0.6$ km s^{-1} (EW = 59 mÅ), both referred to the LSR. These two stars are located at a higher Galactic latitude than HD 166841 and are more distant, but it is worth noting that the first component seen towards HD 143448 is similar within the errors to the one seen towards HD 166841, both in equivalent width and radial velocity.

Despite being located right at the centre of the photospheric lines, there is not enough supporting evidence to attribute this feature to a circumstellar origin. The star is quite distant and there is some evidence of a correlated velocity structure between the feature seen towards HD 166841 and those towards stars in nearby lines of sight. One argument that could favour a circumstellar nature for the feature seen towards HD 166841 is the fact that when IS absorption components are detected towards field stars, generally more than one component is detected, whereas in the case of HD 166841 only one distinctive narrow absorption is observed. Observations of stars
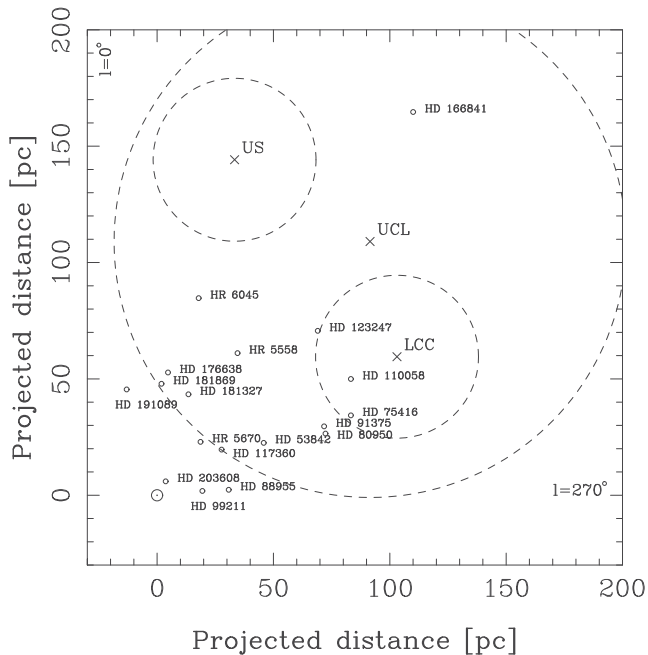
Figure 8. Projection of the positions of the target stars (open circles) on to the Fourth Quadrant of the Galactic plane. The dashed circles indicate the location of the UCL, LCC and US H I shells as described in de Geus, de Zeeuw & Lub (1989), de Geus (1992) and de Zeeuw et al. (1999). The centre of each shell is indicated with a cross. The position of the Sun is located at the origin of the coordinates, and is marked with the ⊙ symbol. The star HD 61950 is located too far away to appear in the plot, positioned near ($x = 330$, $y = 63$).

Table 7. Heliocentric velocity projections of known IS clouds/shells in the direction of the stars presenting narrow absorption features.

Star	LIC (km s^{-1})	G (km s^{-1})	UCL (km s^{-1})	LCC (km s^{-1})
HD61950	0.65	0.91	9.44	–
HD75416	−3.91	−4.01	4.28	–
HD110058	−11.94	−14.16	−5.25	1.92
HD166841	−15.00	−15.81	−9.06	–
HR5558	−21.55	−24.70	−4.93	

with lines of sight closer to HD 166841 than the stars quoted above could help to clarify the nature of HD 166841's narrow absorption feature.

5.3.5 HR 5558

HR 5558 is an A0V spectral standard located 76 pc away from the Sun. We serendipitously detected a narrow absorption feature noticeable in the Na I D lines (EW of 20 and 33 mÅ in the D$_1$ and D$_2$ lines, respectively), and less evident in the Ca II K line. The feature was not detected in the Ca II H line.

There is no correspondence of the radial velocity of the absorption feature with the radial velocity of the star, suggesting that the absorption is of IS origin. This is supported by the low Ca II/Na I ratio derived. Given the diagnostics above, plus the fact that HR 5558 is not known to be a debris disc host star, we conclude that the absorption feature seen towards this star is IS in origin.

6 CONCLUSIONS

We have conducted a search for optical circumstellar absorption lines in the spectra of 16 debris disc host stars. We found no evidence of emission line activity, confirming their more evolved and quiescent evolutionary state. Four stars show narrow absorption features close to the centre the photospheric Ca II and Na I D lines. In addition, similar absorption features were detected in the spectrum of one our spectral standards.

Of the four stars showing narrow absorption features, two are younger than 17 Myr (the other two stars do not have available ages in the literature). This is consistent with the findings of Welsh & Montgomery (2013) in which they note that the stars that exhibit circumstellar gas activity are significantly younger than quiescent systems.

We also find that the systems towards which absorption is detected are all fast rotators. This has been discussed as a possible proxy for detecting gas absorption in debris discs, since it can be indicative of a system seen close to edge-on (Welsh & Montgomery 2013). With the exception of HD 176638, none of the stars with $v \sin i < 140$ km s^{-1} show signatures of gas absorption. We also note that gas absorption is only detected towards A- or late B-type stars, in agreement with previous detections of exocomet bearing systems (e.g. Redfield 2007; Welsh & Montgomery 2013; Eiroa et al. 2016).

The features detected towards HD 61950 and HR 5558 can be almost unambiguously attributed to IS absorption, while in the case of HD 75416 and HD 166841, the association is less clear. The lack of known IS absorption features within the velocity ranges of the lines seen in both HD 75416 and HD 166841 (which coincide with the stellar velocities) leaves open the question of the nature of these features. HD 75416 (η Cha) is known to host an evolved protoplanetary disc, possibly transitioning into the debris disc phase (Sicilia-Aguilar et al. 2009). Re-observation of these two sources in order to search for variability, together with observations of stars in adjacent lines of sight, could help to disentangle the origin of these features. The non-detection of atomic gas absorption towards the CO-rich HD 181237 debris disc system is consistent with this system being seen close to pole-on (Marino et al. 2016).

The most compelling evidence for a circumstellar gas is seen in one of the two velocity components of the absorption seen in the spectrum of HD 110058 (at +12 km s^{-1}). The good agreement with the stellar velocity, the Ca II/Na I column density ratio close to unity, the lack of known IS clouds or shells at the correct velocities in HD 110058's direction, and the fact that the disc is observed close to edge-on strongly suggest that the absorption is caused by atomic gas present in HD 110058's disc. The additional MIKE data provide compelling evidence that the component at +12 km s^{-1} arises in the circumstellar environment of HD 110058.

The detection of optical absorption gas features towards HD 110058, adds to the many similarities with the β Pic system (age, dust fractional luminosity, orientation and presence of both atomic and molecular gas). In the latter, the gas is believed to be of secondary origin, i.e. produced by the release of atomic and molecular species by volatile-rich bodies (Dent et al. 2014; Kral et al. 2016). Future studies of this new β Pic-like system could provide further information on the origins of gas in debris discs.
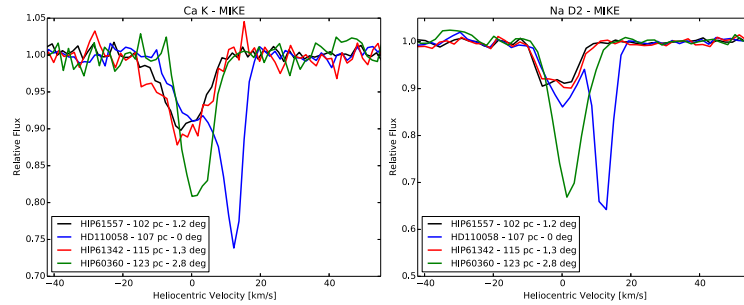
Figure 9. MIKE Ca II spectra towards HD 110058 and reference targets for IS absorption characterization. The parallactic distance to the reference stars and their angular separation from HD 110058 are annotated in the figure.

REFERENCES

Bagnulo S. et al., 2003, The Messenger, 114, 10
Bernstein R., Shectman S. A., Gunnels S. M., Mochnacki S., Athey A. E., 2003, Proc. SPIE, 4841, 1694
Beust H., Vidal-Madjar A., Ferlet R., Lagrange-Henri A. M., 1990, A&A, 236, 202
Beust H. et al., 1998, A&A, 338, 1015
Blaauw A., 1964, ARA&A, 2, 213
Bryden G. et al., 2006, ApJ, 636, 1098
Castelli F., Kurucz R. L., 2004, preprint (astro-ph/0405087)
Crawford I. A., 1991, A&A, 247, 183
Crawford I. A., Spyromilio J., Barlow M. J., Diego F., Lagrange A. M., 1994, MNRAS, 266, L65
Crawford I. A., Beust H., Lagrange A.-M., 1998, MNRAS, 294, L31
Crutcher R. M., 1982, ApJ, 254, 82
de Bruijne J. H. J., Eilers A.-C., 2012, A&A, 546, A61
de Geus E. J., 1992, A&A, 262, 258
de Geus E. J., de Zeeuw P. T., Lub J., 1989, A&A, 216, 44
de Zeeuw P. T., Hoogerwerf R., de Bruijne J. H. J., Brown A. G. A., Blaauw A., 1999, AJ, 117, 354
Dent W. R. F. et al., 2014, Science, 343, 1490
Dunkin S. K., Barlow M. J., Ryan S. G., 1997, MNRAS, 290, 165
Eiroa C. et al., 2016, A&A, 594, L1
Greaves J. S. et al., 2016, MNRAS, 461, 3910
Hales A. S. et al., 2014, AJ, 148, 47
Hobbs L. M., Welty D. E., Lagrange-Henri A. M., Ferlet R., Vidal-Madjar A., 1988, ApJ, 334, L41
Houk N., Smith-Moore M., 1988, Michigan Catalogue of Two-dimensional Spectral Types for the HD Stars, Vol. 4. Department of Astronomy, University of Michigan
Howarth I. D., Price R. J., Crawford I. A., Hawkins I., 2002, MNRAS, 335, 267
Hughes A. M., Wilner D. J., Kamp I., Hogerheijde M. R., 2008, ApJ, 681, 626
Hunter I. et al., 2006, MNRAS, 367, 1478
Kasper M., Apai D., Wagner K., Robberto M., 2015, ApJ, 812, L33
Kelson D. D., 2003, PASP, 115, 688
Kiefer F. et al., 2014a, Nature, 514, 462

Kiefer F. et al., 2014b, A&A, 561, L10
Kóspál Á., Moór A., 2016, IAU Symp., 314, 183
Kral Q., Wyatt M., Carswell R. F., Pringle J. E., Matrà L., Juhász A., 2016, MNRAS, 461, 845
Lagrange-Henri A. M. et al., 1990a, A&AS, 85, 1089
Lagrange-Henri A. M., Beust H., Ferlet R., Vidal-Madjar A., Hobbs L. M., 1990b, A&A, 227, L13
Lagrange-Henri A. M., Gosset E., Beust H., Ferlet R., Vidal-Madjar A., 1992, A&A, 264, 637
Lallement R., Bertin P., 1992, A&A, 266, 479
Lallement R., Ferlet R., Lagrange A. M., Lemoine M., Vidal-Madjar A., 1995, A&A, 304, 461
Lieman-Sifry J. et al., 2016, ApJ, 828, 25
Mamajek E. E., Lawson W. A., Feigelson E. D., 1999, ApJ, 516, L77
Mannings V., Barlow M. J., 1998, ApJ, 497, 330
Marino S. et al., 2016, MNRAS, 460, 2933
Montgomery S. L., Welsh B. Y., 2012, PASP, 124, 1042
Moór A. et al., 2006, ApJ, 644, 525
Moór A. et al., 2011, ApJ, 740, L7
Moór A. et al., 2015, ApJ, 814, 42
Morton D. C., 1991, ApJS, 77, 119
Redfield S., 2007, ApJ, 656, L97
Redfield S., Linsky J. L., 2015, ApJ, 812, 125
Redfield S., Kessler-Silacci J. E., Cieza L. A., 2007, ApJ, 661, 944
Rieke G. H. et al., 2005, ApJ, 620, 1010
Sicilia-Aguilar A. et al., 2009, ApJ, 701, 1188
Slettebak A., 1975, ApJ, 197, 137
Smith B. A., Terrile R. J., 1984, Science, 226, 1421
Smoker J. V., Keenan F. P., Fox A. J., 2015, A&A, 582, A59
Song I., Caillault J.-P., Barrado y Navascués D., Stauffer J. R., 2001, ApJ, 546, 352
Sylvester R. J., Mannings V., 2000, MNRAS, 313, 73
Sylvester R. J., Dunkin S. K., Barlow M. J., 2001, MNRAS, 327, 133
van Leeuwen F., 2007, A&A, 474, 653
Vidal-Madjar A., Lecavelier des Etangs A., Ferlet R., 1998, Planet. Space Sci., 46, 629
Welsh B. Y., Montgomery S., 2013, PASP, 125, 759
Welsh B. Y., Montgomery S., 2016, PASP, 128, 064201
Welsh B. Y., Lallement R., Vergely J.-L., Raimond S., 2010, A&A, 510, A54
Wyatt M. C., 2008, ARA&A, 46, 339

This paper has been typeset from a TEX/LATEX file prepared by the author.